

EVALUATION OF HIGHER ORDER WEIGHT FUNCTIONS BY THE FINITE ELEMENT METHOD

Q. Z. Xiao and B. L. Karihaloo
School of Engineering, Cardiff University,
Queen's Buildings, P O Box 925, Cardiff, CF24 0YF, UK
XiaoQ@Cardiff.ac.uk (QZ Xiao)
KarihalooB@Cardiff.ac.uk (BL Karihaloo)

Abstract

In the evaluation of accurate weight functions for the coefficients of first few terms of the 2D linear elastic crack tip fields and the crack opening displacement (COD) using the finite element method (FEM), singularities at the crack tip and the loading point need to be properly considered. The crack tip singularity can be well captured by a hybrid crack element (HCE), which directly predicts accurate coefficients of first few terms of the linear elastic crack tip fields. A penalty function technique is introduced to handle the point load. Numerical validation will be given.

1. Introduction

Evaluation of the stress intensity factor (SIF, i.e. the first term in the so-called Williams expansion) using weight functions is now a standard method in linear elastic fracture analysis. Such weight functions have been developed for many cracked geometries and loading conditions (see, e.g. Wu and Carlsson [1]; Fett and Munz [2]).

Weight functions for higher order terms of the Williams expansion are also important because of their significance in the fracture process (Chao and Zhang [3]; Fett [4]; Smith et al. [5]; Xiao and Karihaloo [6]). Weight functions for the crack opening displacement (COD) are required in the cohesive-crack-based analysis, as well as in interpreting the size effect of quasi-brittle materials (Karihaloo et al. [7]). Such weight functions are limited in the literature; analytical results are only available for infinite cracked bodies. For practical finite cracked bodies, approximate methods are inevitably used.

In the development of the weight functions, a cracked body has to be analyzed under the application of a point load. If the analytical solution is known for an infinite body with the same loading configuration, the problem for a finite body can be decomposed into an infinite cracked body under the point load, and a finite body with traction free crack faces subjected to tractions on the external boundaries, which cancel out the tractions due to the analytical solution for the infinite body (Xiao and Karihaloo [6]; Fett [8]). The simple boundary collocation method (BCM) can then be used to the finite body with traction free crack faces. However, this method is not accurate for shallow cracks and when the point load is close to the external boundary, as has been shown by Xiao and Karihaloo [9].

The finite element method (FEM), despite its widespread use in the fracture mechanics, is not of direct practical use in the evaluation of weight functions. This is because various crack lengths and different locations of the point load need to be considered, and the crack tip region as well as the neighbourhood of the point load because of stress singularities need to be carefully refined to obtain satisfactory accuracy.

For 2D linear elastic problems, the displacement and stress fields near the crack tip as well as a point load are well known, and several methods for enhancing the FE approximations with the known deformation information have been proposed. Xiao and Karihaloo [9] reviewed briefly the merits and weaknesses of the recent developments with an emphasis on their applicability to predicting higher order terms of the crack tip fields and/or modelling the point load. The hybrid crack element (HCE) of Tong et al. [10] and Karihaloo and Xiao [11] gives the most accurate first few terms of the crack tip field directly without a need for refinement of the crack tip region. This element will be adopted in this study. For the point load, the method for the evaluation of SIFs for cracks and generalized SIFs for re-entrant corners proposed by Seweryn [12] has been improved using the penalty function (PF) approach. This method enhances the FE approximation using the known displacement fields corresponding to a point load and avoids the need for refinement of the mesh in the neighbourhood of the point load. Numerical validation for the accuracy of this treatment of the point load, as well as the coefficients of the crack tip fields and the COD due to wedge forces on the crack faces obtained using the proposed method will be given.

2. Theoretical analysis

If the crack with traction free faces lies on the negative x -axis, and the polar coordinates centred at the crack tip are designated r and ϑ (ϑ is measured counterclockwise from the positive x -axis, Fig. 1a), the displacements and stresses near the tip of the crack subjected to splitting load (mode I) can be expressed as the so-called Williams expansions (see, e.g. [11]):

$$u = \sum_{n=1}^{\infty} \frac{r^{\frac{n}{2}}}{2\mu} a_n \left[\left(\kappa + \frac{n}{2} + (-1)^n \right) \cos \frac{n}{2} \vartheta - \frac{n}{2} \cos \left(\frac{n}{2} - 2 \right) \vartheta \right] \quad (1)$$

$$v = \sum_{n=1}^{\infty} \frac{r^{\frac{n}{2}}}{2\mu} a_n \left[\left(\kappa - \frac{n}{2} - (-1)^n \right) \sin \frac{n}{2} \vartheta + \frac{n}{2} \sin \left(\frac{n}{2} - 2 \right) \vartheta \right] \quad (2)$$

$$\sigma_x = \sum_{n=1}^{\infty} \frac{n}{2} r^{\frac{n}{2}-1} a_n \left[\left(2 + \frac{n}{2} + (-1)^n \right) \cos \left(\frac{n}{2} - 1 \right) \vartheta - \left(\frac{n}{2} - 1 \right) \cos \left(\frac{n}{2} - 3 \right) \vartheta \right] \quad (3)$$

$$\sigma_y = \sum_{n=1}^{\infty} \frac{n}{2} r^{\frac{n}{2}-1} a_n \left[\left(2 - \frac{n}{2} - (-1)^n \right) \cos \left(\frac{n}{2} - 1 \right) \vartheta + \left(\frac{n}{2} - 1 \right) \cos \left(\frac{n}{2} - 3 \right) \vartheta \right] \quad (4)$$

$$\tau_{xy} = \sum_{n=1}^{\infty} \frac{n}{2} r^{\frac{n}{2}-1} a_n \left[\left(\frac{n}{2} - 1 \right) \sin \left(\frac{n}{2} - 3 \right) \vartheta - \left(\frac{n}{2} + (-1)^n \right) \sin \left(\frac{n}{2} - 1 \right) \vartheta \right] \quad (5)$$

where $\mu = E/(2(1+\nu))$ is the shear modulus; $\kappa = 3 - 4\nu$ for plane strain or $\kappa = (3 - \nu)/(1 + \nu)$ for plane stress; E and ν are Young's modulus and Poisson's ratio, respectively. a_1 is related to the mode I SIF K_I as $a_1 = K_I/\sqrt{2\pi}$. The second term in (1-5) corresponds to a in-plane T -stress $\sigma_x = T = 4a_2$.

An edge crack in a finite plate (FSECP) subjected to wedge forces P in Fig. 1a can be decomposed into a semi-infinite crack subjected to wedge forces P in an infinite plate (Fig. 1b) and a FSECP with traction free crack faces (Fig. 1c) [6].

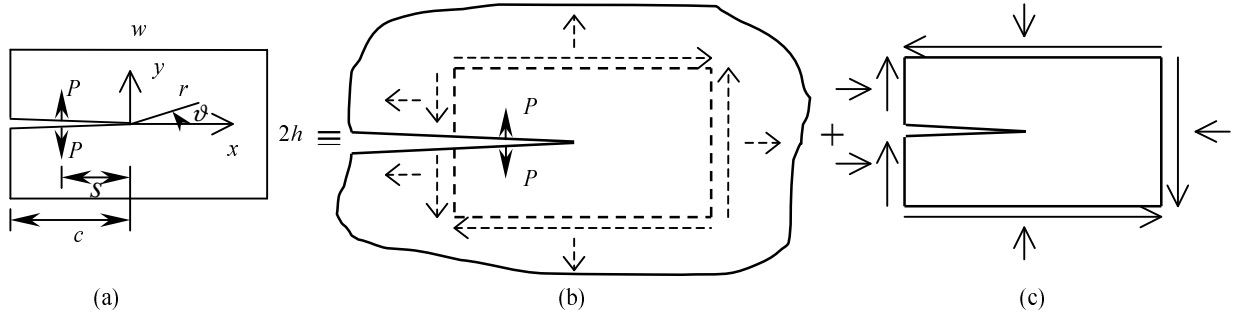


Fig. 1. Decomposition of a finite plate with an edge crack (FSECP) subjected to wedge forces P (a) into an infinite plate with a semi-infinite crack subjected to wedge forces P (b) and a FSECP with traction free crack faces (c).

For the semi-infinite crack in an infinite plate subjected to a pair of wedge forces, P , acting at $(-s, 0)$ (Fig. 1b), the stresses along the extension of the crack line can be written in the form of (3–5) with the coefficients of the first five terms as [6]

$$\hat{a}_1(s) = \frac{P}{\pi} \sqrt{\frac{1}{s}}; \hat{a}_2(s) = 0; \hat{a}_3(s) = -\frac{P}{3\pi} s^{-3/2}; \hat{a}_4(s) = 0; \hat{a}_5(s) = \frac{P}{5\pi} s^{-5/2} \quad (6)$$

The corresponding COD at the location t on the crack face is

$$\hat{\delta}(s, t) = -\frac{4P}{\pi E'} \ln \left| \frac{\sqrt{s} - \sqrt{t}}{\sqrt{s} + \sqrt{t}} \right| \quad (7)$$

where $E' = E$ for plane stress, and $E' = E/(1-\nu^2)$ for plane strain. The coefficients $\hat{a}_1, \hat{a}_2, \dots, \hat{a}_5$, and the COD $\hat{\delta}(s, t)$ for the geometry of Fig. 1b have been distinguished by the symbol ‘ $\hat{}$ ’.

For the FSECP with traction free crack faces (Fig. 1c), the general solution can be expressed in the Williams expansion (1–5). The coefficients $\tilde{a}_n(s; c)$ in (1-5) for this geometry are to be determined by meeting the traction free exterior boundary conditions of Fig. 1a. The corresponding COD at the location t on the crack face is

$$\tilde{\delta}(s, t; c) = v_{r=t, \vartheta=\pi} - v_{r=t, \vartheta=-\pi} = 2v_{r=t, \vartheta=\pi} = \frac{8}{E'} \left(\tilde{a}_1 \sqrt{t} - \tilde{a}_3 t^{3/2} + \tilde{a}_5 t^{5/2} - \dots \right) \quad (8)$$

Weight functions ($P = 1$) for coefficients a_n ($1 \leq n \leq 5$) and COD of the FSECP subjected to wedge forces P (Fig. 1a) can be obtained by combining the relevant terms of the analytical solution (6), (7) of Fig. 1b with the corresponding numerical solutions for Fig. 1c, i.e.

$$a_n(s; c) = \hat{a}_n(s) + \tilde{a}_n(s; c) \quad (9)$$

$$\delta(s, t; c) = \hat{\delta}(s, t) + \tilde{\delta}(s, t; c) \quad (10)$$

Coefficients \tilde{a}_i^1 of a specimen with characteristic size L_1 are related to \tilde{a}_i^2 of another specimen with similar geometry and loading conditions but characteristic size L_2 as

$$\tilde{a}_i^2 = \tilde{a}_i^1 (L_1/L_2)^{i/2} \quad (11)$$

From (7), (8) and (10), for an arbitrary factor k , the COD has the following property

$$\hat{\delta}(ks, kt) = \hat{\delta}(s, t); \tilde{\delta}(ks, kt; kc) = \tilde{\delta}(s, t; c); \delta(ks, kt; kc) = \delta(s, t; c) \quad (12)$$

3. FEs for modeling the point load

In the coordinate system shown in Fig. 2, the displacements in the neighbourhood of the point load are

$$\begin{Bmatrix} u_x \\ v_y \end{Bmatrix} = \begin{bmatrix} (1+\nu)\sin\theta\cos\theta & -(1-\nu)\theta \\ -(1+\nu)\sin^2\theta & -2\ln r \end{bmatrix} \frac{P}{\pi E} + \begin{Bmatrix} 1 \\ 0 \end{Bmatrix} A + \begin{Bmatrix} 0 \\ 1 \end{Bmatrix} B + \begin{Bmatrix} r\cos\theta \\ -r\sin\theta \end{Bmatrix} C \quad (13)$$

where A , B , and C are constants depending on the remote boundary conditions. The corresponding stresses are

$$\sigma_r = -\frac{2P\cos\theta}{\pi r}, \quad \sigma_\theta = \tau_{r\theta} = 0 \quad (14)$$

Since the strain energy is unbounded in the neighbourhood of the point load, the above known deformation fields (13) cannot be used to enrich the FE approximation via most methods appropriate for corners or crack tips. For example, if the partition of unity method (PUM) is used, the entries in the system stiffness matrix corresponding to the singular fields above will be very large (akin to penalty function terms). As a result the corresponding coefficient $P/(\pi E)$, if it is treated as an unknown variable, will vanish. The results cannot be improved even when the known amplitude $P/(\pi E)$ is enforced as a prescribed displacement. This has been confirmed by numerical results. These results will, however, not be presented here for brevity. The DtN method, especially its extension by Seweryn [12], seems most appropriate for point loads. A disadvantage of Seweryn's method is that all the nodes which enforce the known analytical solution have to be numbered consecutively, i.e., as the first or final block of the nodes. A transformation to the system stiffness matrix is required. After transformation, the total degrees of freedom of the system will change. This complicates its practical implementation. It is improved as follows in the present paper.

The set of unknowns of the discrete system (i.e. the nodal displacement vector) is expanded to include the coefficients in the displacement fields (13) of the neighbourhood of a point load. The amplitude $P/(\pi E)$ in (13) is also treated as an unknown coefficient in the beginning, and later enforced as a prescribed displacement. The displacement field (13) acts as constraints on the displacements at nodes surrounding the loading point in the expanded unknown displacement vector. These constraints are enforced through a PF approach, in a similar manner to the enforcement of periodic boundary displacement conditions in a homogenization problem (Karihaloo et al. [13]). Note that integration of singular integrands is avoided as no singular functions are used explicitly in the FE formulation. In the computations to follow, the first ring of nodes surrounding the loading point will be considered, and a penalty factor of $10^3 E$ will be used to guarantee convergence of numerical solutions.

Since the PF method has been used, the discretized system of equations will be badly scaled. We have used the HSL packages MC30 and MA57 to scale and solve the system.

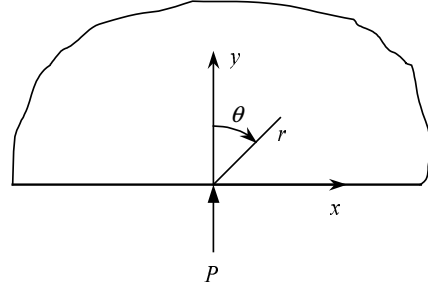


Fig. 2. A concentrated vertical force P per unit thickness acting on a horizontal straight boundary of an infinite plate.

4. Numerical tests

4.1 Tests on the PF approach

In order to check the accuracy of the implementation of the point load, a finite plate shown in Fig. 3a subjected to a point load is analysed. The prescribed boundary displacements are in the form of (13) with coefficients

$$A = C = 0, \quad B = \frac{2P}{\pi E} \ln 10 \quad (15)$$

These fields are actually the exact displacements in the whole plate. The load P is assumed to be 1 per unit thickness. Young's modulus E is set at 1, and Poisson's ratio ν at 0.25. The units of loading (Fig. 3a) are consistent with that of E . A state of plane stress is considered with thickness assumed to be 1. Only one half of the plate needs to be considered because of symmetry. The FE mesh corresponding to a 10×10 uniform division is shown in Fig. 3b. The displacements at the first ring of nodes surrounding the point load, as shown in Fig. 3b, will be used to validate the accuracy of different methods. The bilinear isoparametric element Q4 and the PS element of Pian and Sumihara [14] are used in the tests. 2×2 Gauss quadrature is employed for their formulation. The displacements at the three chosen nodes are compared in Table 1 with the exact results. The exact displacements are calculated from (13) with coefficients (15). It is seen from Table 1 that without proper consideration of the singularity at the loading point, neither Q4 nor PS element gives displacements close to the exact solution with the relatively coarse mesh of Fig. 3b. On the other hand, with the use of the PF approach discussed above, highly improved displacements have been obtained with both Q4 and PS elements. Obviously, the high accuracy of the displacements at the first ring of nodes surrounding the point load guarantees the accuracy of far fields.

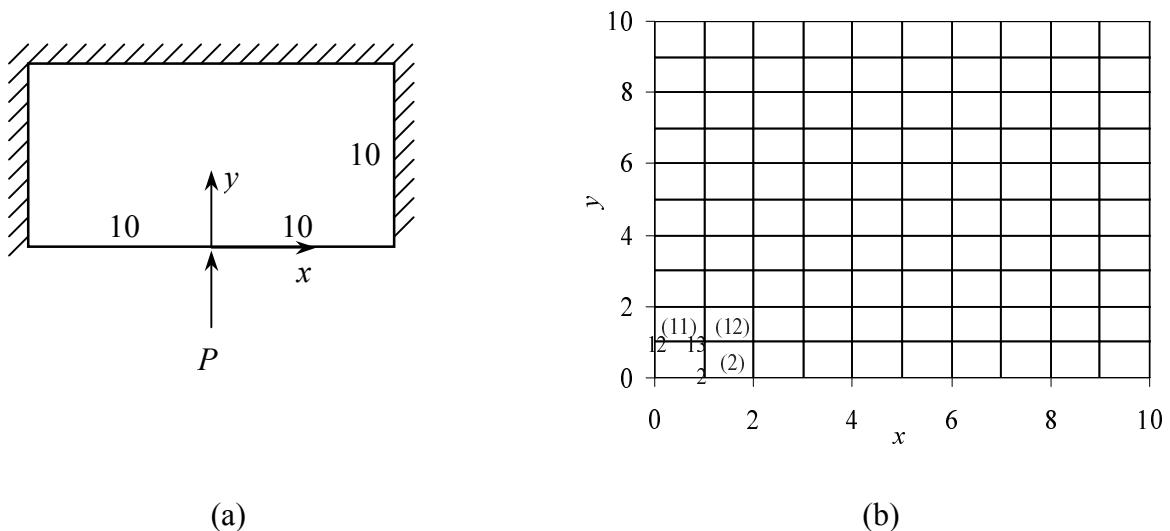


Fig. 3. (a) A finite plate subjected to a point load. (b) FE mesh for one half of the plate corresponding to a 10×10 uniform division. The nodes 2, 12, 13 and the elements (2), (11), (12) surround the location of point load at (0, 0).

TABLE 1. Displacements at nodes surrounding the point load.

Method	Node 2 (1, 0)*		Node 12 (0, 1)		Node 13 (1, 1)	
	u_x	v_y	u_x	v_y	u_x	v_y
Q4	-0.3356	1.0104	0	1.4333	0.0547	1.0746
Q4 + PF (1st term)	-0.3429	1.0813	0	1.4473	0.0116	1.0598
Q4 + PF (all terms)	-0.3750	1.0679	0	1.4659	0.0115	1.0464
PS	-0.3715	0.9611	0	1.4196	0.0834	1.1090
PS + PF (1st term)	-0.3573	1.0848	0	1.4651	0.0116	1.0633
PS + PF (all terms)	-0.3750	1.0679	0	1.4659	0.0115	1.0464
Exact	-0.3750	1.0680	0	1.4659	0.0114	1.0463

* Coordinates of the node.

4.2. A wedge-splitting (WS) specimen

In the following, a WS specimen with $W = 100\text{mm}$, $d_n = 15\text{mm}$, $f = 30\text{mm}$, and $e = 35\text{mm}$ (Fig. 4) subjected to wedge forces will be analyzed. The crack length to depth ratio $\alpha = c/(W - d_n) = 0.1$ and $s/c = 0.92$. Only one half of the specimen needs to be considered because of symmetry. The load P is assumed to be 1 per unit thickness.

A 21-node HCE (the first 39 terms in (1-5) are included in the element formulation) together with a relatively fine discretisation of the remainder of the body will be used. Three-point Gauss integration is used for each side (segment) of the HCE. The PS element [14] is used in conjunction with the HCE, and the traction free conditions on the exterior boundary are exactly satisfied using the special hybrid stress boundary element HBE (Xiao et al. [15]). 2×2 and 3×3 Gauss quadratures are employed for the formulation of PS and HBE, respectively. The FE mesh used in the computations is shown in Fig. 5a. The coordinate system used is the same as that shown in Fig. 4. The HCE is symmetric about the y -axis; it is rectangular with its length (in x -direction) twice that of its height (in y -direction). The scaled coordinate axes are also included in Fig. 5a to show the location of the HCE relative to the rest of the mesh. The mesh patterns surrounding the HCE and at the neighbourhood of the point load are shown in Fig. 5b and 5c for clarity. The PF approach is used to treat the loading point. In the computations Young's modulus E is set at 1, and Poisson's ratio ν at 0.25. The units of loading (Fig. 4) are consistent with that of E . A state of plane stress is considered with thickness assumed to be 1.

The specimen was also analyzed with refinement at the location of the point load, as shown in Fig. 5d, and without using the PF approach. The results for the coefficients of the first five terms are compared in Table 2; and the CODs are compared in Fig. 6. Their excellent agreement confirms the high accuracy of the numerical results obtained above. With the refined mesh, numerical results show that the coefficients a_n as well as the COD do not change irrespective of whether or not the FE approximation is enriched with the PF approach, since the results are highly accurate.

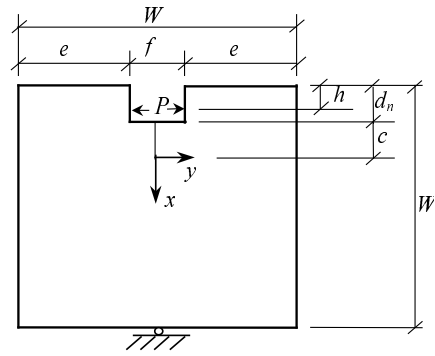
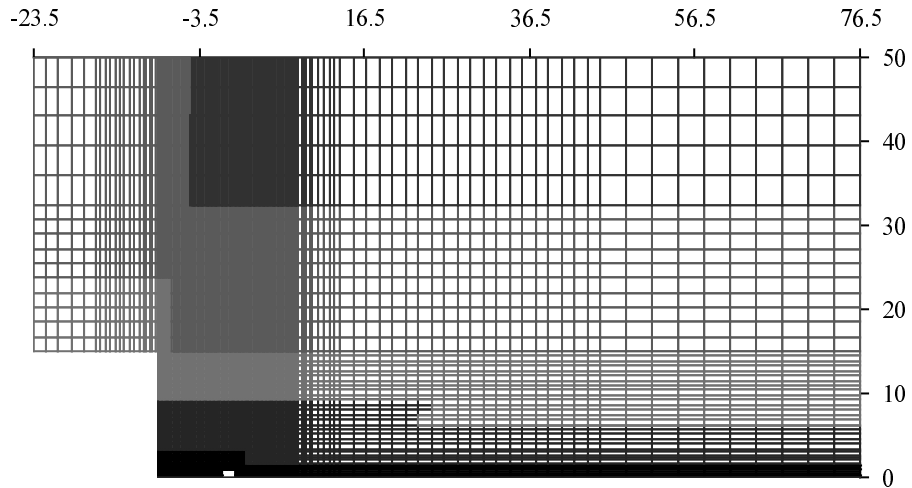
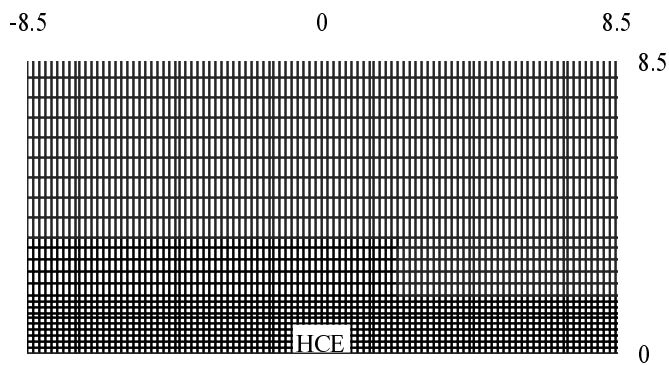


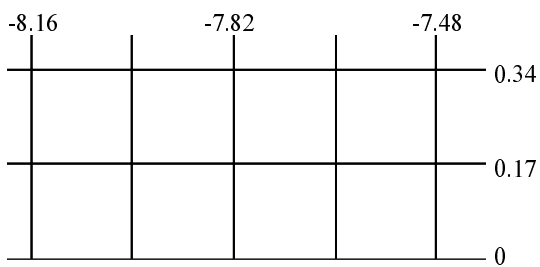
Fig. 4. WS specimen.



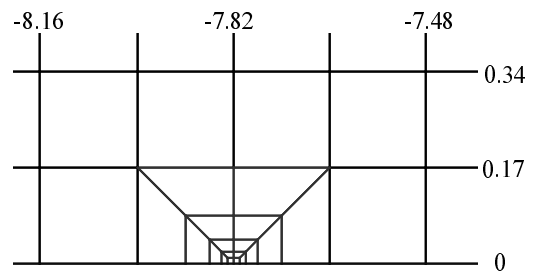
(a)



(b)



(c)



(d)

Fig. 5. (a) FE mesh; (b) Mesh pattern surrounding the HCE; (c) Uniform mesh near the loading point; (d) Refined mesh near the loading point.

TABLE 2. The coefficients $a_1 \sim a_5$ obtained with different treatment of the loading point.

Treatment	a_1	$a_2 \times 10$	$a_3 \times 10$	$a_4 \times 10^2$	$a_5 \times 10^2$
PF	0.22726	0.28102	-0.11939	-0.20276	0.10036
Refinement	0.22728	0.28114	-0.11944	-0.20283	0.10044

4. Conclusions

The penalty function approach introduced in this paper simplifies the practical implementation of the method by Seweryn [12] without any loss of its accuracy. This method gives highly accurate fields at the neighbourhood of a point load without the use of a very fine mesh. Using this method to capture the elastic field of the point load and the HCE to capture the elastic field of a crack tip, the FEM becomes a powerful tool for the evaluation of 2D weight functions for the SIF, coefficients for higher order terms and the COD.

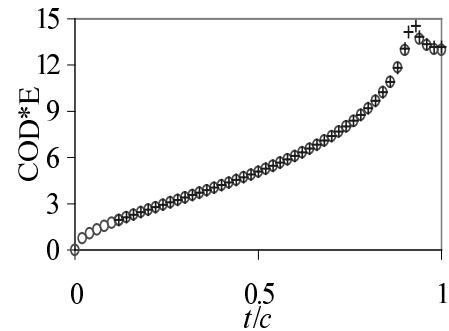


Fig. 6. COD for $\alpha = 0.1$, $s/c = 0.92$.

○ PF + Refinement

Acknowledgement

Financial support from UK EPSRC under grant number GR/R 11339 is gratefully acknowledged. Access to HSL packages MC30 and MA57 was kindly provided by the Numerical Analysis Group at Rutherford Appleton Laboratory.

References

1. Wu, X.R. and Carlsson, A.J., *Weight Functions and Stress Intensity Factor Solutions*, Pergamon, Oxford, 1991.
2. Fett, T. and Munz, D., *Stress Intensity Factors and Weight Functions*, Computational Mechanics Publications, Southampton, 1997.
3. Chao, Y.J. and Zhang, X., Constraint effect in brittle fracture, In *ASTM STP 1296, Fatigue and Fracture Mechanics 27*, edited by R. Piascik, 1997, 41-60.
4. Fett, T., *Engng. Fract. Mech.*, **57**, 365-373, 1997.
5. Smith, D.J., Ayatollahi, M.R. and Pavier, M.J., *Fatigue Fract. Engng. Mater. Struct.*, **24**, 137-150, 2001.
6. Xiao, Q.Z. and Karihaloo, B.L., *Engng. Fract. Mech.*, **69**, 959-981, 2002.
7. Karihaloo, B.L., Abdalla, H.M. and Xiao, Q.Z., *Engng. Fract. Mech.*, **70**, 979-993, 2003.
8. Fett, T., *T-stress Solutions and Stress Intensity Factors for 1-D Cracks*, VDI Verlag, Düsseldorf, 2002.
9. Xiao, Q.Z. and Karihaloo, B.L., FEM for evaluation of weight functions for SIF, COD and higher order coefficients with application to a typical wedge splitting specimen, *Int. J. Fract.*, 2004 (in press).
10. Tong, P., Pian, T.H.H. and Lasry, S.J., *Int. J. Numer. Meth. Engng.*, **7**, 297-308, 1973.
11. Karihaloo, B.L. and Xiao, Q.Z., *Engng. Fract. Mech.*, **68**, 1609-1630, 2001.
12. Seweryn, A., *Int. J. Solids Struct.*, **39**, 4787-4804, 2002.
13. Karihaloo, B.L., Xiao, Q.Z. and Wu, C.C., *Comput. Struct.*, **79**, 1645-1660, 2001.
14. Pian, T.H.H. and Sumihara, K., *Int. J. Numer. Meth. Engng.*, **20**, 1685-1695, 1984.
15. Xiao, Q.Z., Karihaloo, B.L. and Williams, F.W., *Engng. Fract. Mech.*, **63**, 1-22, 1999.